Early identification of antigen-specific immune responses in vivo by [^{18}F]-labeled 3′-fluoro-3′-deoxy-thymidine ([^{18}F]FLT) PET imaging

Erik H. J. G. Aarntzen[a,b], Mangala Srinivas[a,1], Johannes H. W. De Wilt[c,1], Joannes F. M. Jacobs[a,b,d], W. Joost Lesterhuis[a,b], Albert D. Windhorst[e], Esther G. Troost[f], Johannes J. Bonenkamp[c], Michelle M. van Rossum[g], Willeke A. M. Blokx[h], Roel D. Mus[i], Otto C. Boerman[j], Cornelis J. A. Punt[b,2], Carl G. Figdor[a], Wim J. G. Oyen[j], and I. Jolanda M. de Vries[a,b,3]

Departments of [a]Tumor Immunology, [b]Medical Oncology, [c]Surgery, [d]Laboratory Medical Immunology, [f]Radiotherapy, [g]Dermatology, [h]Pathology, [i]Radiology, and [j]Nuclear Medicine, Radboud University Nijmegen Medical Centre, 6500 HB, Nijmegen, The Netherlands; and [e]Department of Nuclear Medicine and PET Centre, Free University (VU) Medical Centre, 1007 MB, Amsterdam, The Netherlands

Edited by Owen N. Witte, Howard Hughes Medical Institute, University of California, Los Angeles, CA, and approved September 23, 2011 (received for review August 16, 2011)

Current biomarkers are unable to adequately predict vaccine-induced immune protection in humans with infectious disease or cancer. However, timely and adequate assessment of antigen-specific immune responses is critical for successful vaccine development. Therefore, we have developed a method for the direct assessment of immune responses in vivo in a clinical setting. Melanoma patients with lymph node (LN) metastases received dendritic cell (DC) vaccine therapy, injected intranodally, followed by [^{18}F]-labeled 3′-fluoro-3′-deoxy-thymidine ([^{18}F]FLT) PET at varying time points after vaccination. Control LNs received saline or DCs without antigen. De novo immune responses were readily visualized in treated LNs early after the prime vaccination, and these signals persisted for up to 3 wk. This selective [^{18}F]FLT uptake was markedly absent in control LNs, although tracer uptake in treated LNs increased profoundly with as little as 4.5×10^5 DCs. Immunohistochemical staining confirmed injected DC dispersion to T-cell areas and resultant activation of CD4$^+$ and CD8$^+$ T cells. The level of LN tracer uptake significantly correlates to the level of circulating antigen-specific IgG antibodies and antigen-specific proliferation of T cells in peripheral blood. Furthermore, this correlation was not observed with [^{18}F]-labeled fluoro-2-deoxy-2-D-glucose. Therefore, [^{18}F]FLT PET offers a sensitive tool to study the kinetics, localization, and involvement of lymphocyte subsets in response to vaccination. This technique allows for early discrimination of responding from nonresponding patients in anti-cancer vaccination and aid physicians in individualized decisionmaking.

individualized treatment | molecular imaging | immune monitoring | cellular therapy

The field of vaccination has expanded over the last few years to include the development of therapeutic vaccines against infectious diseases such as AIDS (1, 2) and tuberculosis (3), as well as conditions such as cancer (4, 5). In particular, antigen-specific immunotherapy has recently progressed through the development of effective therapeutic vaccinations in advanced melanoma (6–8) and prostate cancer (5). Antigen-specific immune responses in cancer patients can also be induced by exploiting autologous dendritic cells (DCs) that are "educated" ex vivo; i.e., DCs that are appropriately activated and loaded with tumor antigens (9). DCs are the most potent antigen-presenting cells of the immune system and play a central role in the induction and maintenance of antigen-specific immunity (10). These cells capture and process antigen and migrate to the lymph nodes (LNs), where they present the antigen to the adaptive arm of the immune system, inducing antigen-specific T- and B-cell responses. This vaccine-induced immune protection cannot be adequately detected in humans, because most therapeutic vaccines have been characterized only in animal models (3, 11). The detection of vaccine-inducted immune responses in vivo using a clinically applicable means is critical for the optimization of novel immunotherapies. Thus, we developed a technique for the direct assessment of immune responses in vivo during therapeutic vaccination.

Positron emission tomography (PET) is a widely available, highly sensitive imaging modality for the in vivo visualization and quantification of molecular processes at a cellular level. Furthermore, whole body imaging allows localization in a longitudinal fashion. These features are necessary to measure immune responses by quantification of the low numbers of proliferating T and B cells early after vaccination in relevant LNs. Thus far, investigators have mainly exploited [^{18}F]-labeled fluoro-2-deoxy-2-D-glucose ([^{18}F]FDG) for PET imaging of proliferating cells, based on the increased glucose metabolism of these cells. Recently, novel tracers have been developed that facilitate imaging of other cellular processes: [^{18}F]-labeled 3′-fluoro-3′-deoxy-thymidine ([^{18}F]FLT) was designed as a tracer for cell proliferation (12) and is increasingly being applied in oncology. However, it has been recognized that enhanced nucleoside demand is not restricted to tumor cells (13). A successful vaccination results in the proliferation of activated lymphocytes in a highly controlled manner within LNs. This proliferation is accompanied by a large metabolic switch in lymphocytes (14) and could serve as a marker of immune responsiveness.

We hypothesized that PET imaging, exploiting [^{18}F]FLT, can specifically detect highly proliferative immune cell responses in proximal LNs upon vaccination and, thus, would allow in vivo assessment of vaccine-induced antigen-specific T- and B-cell responses. Such a "detection system" would allow early discrimination of responding patients and, therefore, aid physicians in individualized decisionmaking.

Results

[^{18}F]FLT PET Visualizes the Immune Response Early After Vaccination. To evaluate whether the [^{18}F]FLT PET signal of proliferating T and B cells colocalized with antigen-loaded DCs, we labeled the

Author contributions: E.H.J.G.A., C.J.A.P., C.G.F., W.J.G.O., and I.J.M.d.V. designed research; E.H.J.G.A., J.H.W.D.W., J.F.M.J., A.D.W., E.G.T., J.J.B., M.M.v.R., W.A.M.B., R.D.M., O.C.B., C.J.A.P., C.G.F., W.J.G.O., and I.J.M.d.V. performed research; E.H.J.G.A., M.S., W.J.L., O.C.B., C.J.A.P., C.G.F., W.J.G.O., and I.J.M.d.V. analyzed data; and E.H.J.G.A., M.S., J.F.M.J., W.J.L., O.C.B., C.J.A.P., C.G.F., W.J.G.O., and I.J.M.d.V. wrote the paper.

The authors declare no conflict of interest.

This article is a PNAS Direct Submission.

Freely available online through the PNAS open access option.

[1]M.S. and J.H.W.D.W. contributed equally to this work.

[2]Present address: Academic Medical Center, Department of Medical Oncology, 1105 AZ, Amsterdam, The Netherlands.

[3]To whom correspondence should be addressed. E-mail: j.devries@ncmls.ru.nl.

This article contains supporting information online at www.pnas.org/lookup/suppl/doi:10.1073/pnas.1113045108/-/DCSupplemental.

cells ex vivo with [^{111}In]oxine and superparamagnetic iron oxide (SPIO). Planar scintigraphy was performed immediately after PET/computed tomography (CT) scanning to localize and quantify the [^{111}In]-labeled DCs (Fig. S1). Three days after vaccination, up to four LNs were revealed with retention of [^{18}F]FLT (Fig. 1*A*). The scintigraphic images demonstrated that the PET signal intensity increased only in those LNs that contained antigen-loaded [^{111}In]-labeled DCs (Fig. 1*B*). Profound [^{18}F]FLT uptake was observed even when very low numbers (4.5×10^5 cells) of antigen-loaded DCs were present. Immunohistochemical staining of the LNs revealed the presence of SPIO-labeled DC in the T-cell areas and the activation of $CD4^+$ and $CD8^+$ T cells (Fig. 1 *C* and *D*).

[^{18}F]FLT PET Signal Requires Antigen-Loaded DCs. We observed a significant increase in [^{18}F]FLT signal early after the first vaccination (Fig. 1 *E* and *F*), indicating that de novo immune responses are readily visualized. Vaccinated LNs remained positive up to 3 wk after the last vaccination (Fig. 1 *G* and *H*). Bone marrow uptake served as internal positive control. Four patients underwent sequential scanning after vaccination. We observed a pronounced increase in [^{18}F]FLT signal exclusively in vaccinated LNs from days 3 to 6 after vaccination in three of four patients (Fig. 1 *I* and *L*).

We observed a further increase in [^{18}F]FLT accumulation ($P < 0.05$) in LNs of patients who received three subsequent intranodal vaccinations, but not in control LNs who were not injected, injected with saline, or injected with DC not loaded with antigen (Fig. 2 *A* and *C*). Therefore, the observed increase in PET signal upon vaccination cannot be attributed solely to the effect of tissue damage by intranodal injection or to the presence of DCs alone, but it requires the presence of antigen. Interestingly, in one patient who did not detect PET signal in LN upon vaccination, the vaccine included the melanoma-associated antigens but not keyhole limpet hemocyanin (KLH). Thus, these data support the notion that the measured [^{18}F]FLT signal is antigen-specific.

[^{18}F]FLT PET Signal Correlates with in Vitro Monitoring Assays. To validate our findings, we compared tracer retention in the LNs with the presence of antigen-specific T- and B-cell responses in peripheral blood samples taken at the time of imaging. We observed a significant correlation between [^{18}F]FLT accumulation and the level of circulating KLH-specific IgG antibodies and KLH-specific proliferation of T cells (Fig. 2 *D* and *E*). In one patient (circle), we observed high [^{18}F]FLT uptake without apparent KLH-specific T-cell proliferation. This patient not only showed exceptionally high KLH-specific IgG antibodies in the serum, but also profound levels of IgA and IgM antibodies, indicating that in this case, the [^{18}F]FLT signal most likely reflects vigorous B-cell proliferation. Another patient (open square) exhibited modest B-cell responses but pronounced T-cell proliferation against KLH. Together from these observations, we conclude that accumulation of [^{18}F]FLT in the vaccinated LNs reflects the sum of both antigen-specific T and antigen-specific B-cell responses. This correlation is specific to the FLT tracer because it was not observed with [^{18}F]FDG.

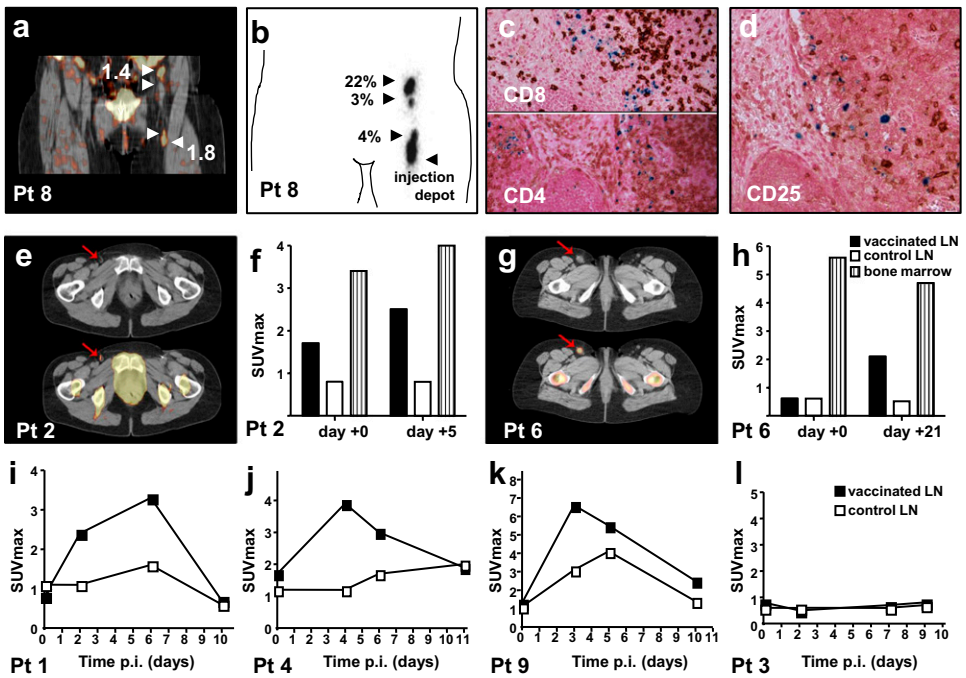

Fig. 1. [^{18}F]FLT PET visualizes the immune response after vaccination. (*A*) Three days after intranodal delivery of the [^{111}In]/SPIO-labeled and antigen-loaded DC, [^{18}F]FLT PET/CT scan was performed and showed tracer retention in the injected and three draining LNs. (*B*) Immediately before the PET/CT scan, the same LNs were visualized by scintigraphy, containing 4%, 3%, and 22% of the injected radioactivity. (*C* and *D*) During the same day, a radical LN dissection was performed and [^{111}In]-DC containing LNs were identified with a gamma probe. Immunohistochemical analyses of these LNs demonstrated a close interaction between injected SPIO-labeled DC and $CD8^+$ T cells, resulting in increased expression of activation marker CD25. (*E* and *F*) To show that de novo immune responses can also be imaged with [^{18}F]FLT, we performed [^{18}F]FLT PET scans in one patient after the prime vaccination (pt 2). At day 5 after vaccination, [^{18}F]FLT signal had increased from SUV_{max} 1.7–2.5, whereas the control lymph node that received vaccination with DC not loaded with antigen did not show an increase in [^{18}F]FLT signal (SUV_{max} 0.9–0.8). (*G* and *H*) In patient 6, who received multiple vaccinations, a sustained [^{18}F]FLT signal was detected up to 3 wk after the last vaccination, but not in the nonvaccinated control LN. (*I–L*) To find the optimal time point for [^{18}F]FLT PET imaging, sequential [^{18}F]FLT PET/CT scans were performed in four patients. We observed a profound increase in [^{18}F]FLT signal in vaccinated LNs (filled squares) but not in control LNs (open squares) between days 3 and 6 after injection with antigen-loaded DC. However, patient 3 received vaccination with DC loaded with tumor-antigen but not the control-antigen KLH. All patients received no other vaccinations 6 mo before imaging.

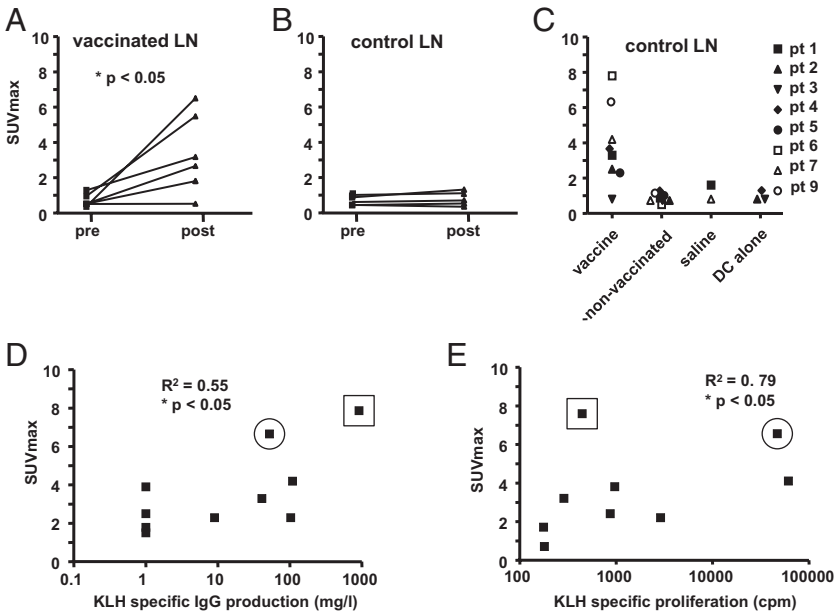

Fig. 2. Increased [^{18}F]FLT PET signal directly correlates to antigen-specific immune responses. (*A*) A significant increase in [^{18}F]FLT signal ($P < 0.05$) was detected in LNs after three intranodal vaccinations, except in one patient (pt 3). (*B*) In contrast, in control LNs, no increase in tracer retention was observed. (*C*) Control LNs consisted of LNs at the contralateral side, either nonvaccinated LN or LN vaccinated with saline or DCs not loaded with antigen. An increase of [^{18}F]FLT signal was not observed in any of these cases. (*D*) Peripheral blood samples at the time point of the scan showed a significant correlation between the level of KLH-specific IgG antibodies and the intensity of [^{18}F]FLT uptake in the LNs, $P < 0.05$. (*E*) Proliferation of peripheral blood mononuclear cells upon stimulation with KLH demonstrated a clear correlation between the intensity of [^{18}F]FLT signal and the KLH-specific proliferation in vitro, $P < 0.05$. One patient (double square) showed high [^{18}F]FLT uptake (SUV_{max} 7.8) without accompanying KLH specific proliferation (403 ± 76 cpm) but showed pronounced humoral response to KLH (KLH IgG 918 mg/L), involving also KLH-specific IgA and IgM. In a second patient (circle), the observed [^{18}F]FLT PET signal (SUV_{max} 6.6) resulted from a modest KLH-specific IgG response (KLH IgG 118 mg/L) and a pronounced KLH-specific proliferation (45,030 ± 12,996 cpm).

Discussion

We demonstrate that [^{18}F]FLT PET can be used to directly monitor antigen-specific immune responses in vivo shortly after therapeutic vaccination, because it offers a sensitive tool to study the kinetics and localization of induction of antigen-specific lymphocyte activation upon vaccination with antigen-loaded autologous DCs.

For vaccination strategies in preventive settings, the established in vitro assays for proliferative and humoral responses are sufficient to predict adequate immunity. However, for a number of novel vaccination strategies that are designed as therapeutic intervention, no such established assays exist. To the contrary, for therapeutic vaccines that target major infectious diseases such as HIV, tuberculosis, malaria, or malignancies, the lack of tools to predict adequate immunity hampers translation of these vaccines to the clinic.

We took the opportunity of our vaccination protocols that provide a unique setting in which we can control all elements required for a successful immune response; the antigen presenting cell is labeled and tracked in vivo, loaded with known antigens, and delivered at the specific immune reactive site. Furthermore, the induced lymphocyte responses can be measured with established and well-validated assays. We used this system as a model to systematically investigate the application of noninvasive in vivo nuclear imaging modality to evaluate antigen-specific immune responses upon therapeutic vaccination.

In recently published large phase III trials, it has been demonstrated that immunotherapies can be effective even in advanced cancer patients. Both antigen-specific (5, 7) and nonantigen specific agents (6) have been approved by the Food and Drug Administration. Considering the amount of effort poured into the development of these novel agents, PET-based monitoring will advance our knowledge of the immunological processes that precede the failure or success of novel immunotherapies. Furthermore, it should vastly improve efficient application by aiding in individualized decisionmaking.

Most anti-cancer vaccines aim at inducing tumor-specific cytotoxic $CD8^+$ T-cell responses. However, tumor-specific $CD8^+$ T-cell responses occur at low precursor frequencies and might therefore contribute less to LN reactivity than vigorous KLH-specific responses (8). To this end, we injected three patients with DCs loaded with KLH, but not with tumor antigen. Interestingly, we measured markedly increased [^{18}F]FLT signals that cannot solely be attributed to KLH, because control vaccination with KLH-loaded DC in contralateral LNs induced only a modest [^{18}F]FLT signal (Fig. S2). The challenge we face is to further improve immune response imaging in vivo and find tracers that are specific for different lymphocyte populations. Recently, in a preclinical model of mice challenged with an immunogenic sarcoma, [^{18}F]FDG accumulated mainly in cells of the innate immune system, whereas 2-fluoro-D-(arabinofuranosyl)-cytosine accumulated predominantly in $CD8^+$ T cells (15). Our findings that [^{18}F]FDG signal intensity does not correlat with immune reactivity (Fig. S3) indicates that targeting glucose metabolism is not specific for antigen-specific immune activation. Hence, we have shown that [^{18}F]FLT is a sensitive and specific PET tracer for monitoring lymphocyte activation after DC vaccine therapy in a clinical setting.

Methods

Patients and Treatment Schedule. The presented data result from side studies in two clinical trials in melanoma patients with regional lymph node metastases who are scheduled for radical lymph node dissection (ClinicalTrials.gov no. NCT00243594 and NCT00243529). Eligibility criteria included stage III melanoma according to the 2001 American Joint Committee on Cancer Staging criteria (16), planned regional lymph node dissection (RLND) for lymph node metastases or interval <2 mo after RLND, HLA-A2.1 phenotype, melanoma expressing gp100 and tyrosinase, and World Health Organization performance status 0 or 1. Additional eligibility criteria have been described (17). The study was approved by our Regional Review Board, and written informed consent

was obtained from all patients. In total, 14 patients were included for additional imaging studies.

The vaccine consisted of autologous mature DCs, pulsed with tumor-associated antigens and KLH. KLH is a highly immunogenic antigen that serves as a surrogate marker for immune competence and as a nonspecific T helper cell stimulus. Similar DCs, but not loaded with KLH or tumor antigen, or sterile saline served as control vaccination. All injections were directly to the LN (intranodally) by a highly experienced radiologist under ultra-sound guidance.

All patients received three intranodal vaccinations at a biweekly interval; patients who remained free of disease progression were eligible for two maintenance cycles at 6-mo intervals with the same schedule. One or two days before RLND, patients received one extra vaccination with DCs labeled with [^{111}In]-oxine and superparamagnetic iron oxide (SPIO) for cell tracking studies in the region that was to be resected (18).

Dendritic Cell Vaccine. Monocytes were enriched from leukapheresis as described (19) and cultured in the presence of interleukin (IL)-4 an granulocyte-macrophage colony stimulating factor to induce differentiation to DC phenotype. DCs were matured with a mixture of proinflammatory cytokines consisting of IL-1β, IL-6, and TNF-α supplemented with prostaglandin E_2 for 48 h. This procedure gave rise to mature DCs meeting the release criteria (20). DCs were pulsed with the HLA class I gp100-derived peptides gp100:154–167, gp100:280–288, and the tyrosinase-derived peptide tyrosinase:369–376 directly after harvesting or thawing. Alternatively, mature DCs were electroporated with mRNA encoding gp100 or tyrosinase (21). Peptide pulsing or mRNA electroporation was performed under good manufacturing practice conditions. More detailed description of the ex vivo culture methods are provided in *SI Methods*. Cells were resuspended in 0.1 mL of saline for intranodal injection.

PET Imaging. PET/CT scans were performed at varying time points after vaccination (Table S1). Patients were instructed to drink 1 L of water and received 10 mg of furosemide i.v. to stimulate urinary tracer excretion. Emission images were acquired 1 h after i.v. injection of 250 MBq [^{18}F]FLT. The images were corrected for attenuation by using low-dose CT and reconstructed by using the ordered-subsets expectation maximization algorithm. Low-dose CT scan was used for anatomical correlation. The image sets were reviewed in consensus by two observers. 3D regions of interest were placed manually over LNs by using a dedicated software program. Maximum standardized uptake values (SUV_{max}) were calculated for visible LNs of interest, according to the following formula: SUV = radioactivity concentration in tissue (Bq/kg)/[injected dose (Bq)/patient weight (kg)]. Bone marrow SUV_{max} in the proximal part of the femoral bone served as internal positive control.

In Vitro Immune Monitoring. Antibodies against KLH were measured in the serum of vaccinated patients by using ELISAs (17). Microtiter plates were coated with KLH, and different concentrations of patient serum were allowed to bind. After extensive washing, patient antibodies were detected with mouse anti-human IgG, IgA, or IgM antibodies labeled with horseradish peroxidase; 3,3′-5,5-tetramethyl-benzidine was used as a substrate and plates were measured in a microtiter plate reader. An isotype-specific calibration curve for the KLH response was included in each microtiter plate. Cellular responses against KLH were measured in a proliferation assay; 1×10^5 peripheral blood mononuclear cells taken at time points of scanning were plated per well either in the presence of KLH or without. After 4 d of culture, 1 μCi per well of [^{3}H]thymidine was added, and incorporation was measured in a β-counter.

[^{111}In] Labeling and Scintigraphy. DC were incubated with [^{111}In]-oxine for 15 min at room temperature. In vivo planar scintigraphic images were acquired with a gamma camera equipped with medium energy collimators, at day 0 and 48 h later. Migration was quantified by region-of-interest analysis of the individual nodes visualized on the images and expressed as the relative fraction of [^{111}In]-labeled DC that had migrated from the injection depot.

SPIO Labeling and Immunohistochemistry. SPIO was added 3 d after onset of DCs culturing. The iron content was determined to be 10–30 pg of iron per cell in this standardized procedure (22) without affecting the viability. Sections (10 μm) of the resected LNs were stained with 2% potassium hexacyanoferrate (II)-trihydrate in 0.2 M HCl for 15 min and counterstained with 0.05% nuclear fast red in 5% aluminum sulfate. Immunohistochemistry was performed by using antibodies against CD4, CD8, and CD25. The slides were stained with Prussian Blue to detect SPIO-labeled cells.

Statistical Analysis. The two-tailed paired Student *t* test was applied for comparison of before and after vaccination PET signals of LNs and bone marrow. Correlations between SUV_{max} of PET signal in LN and KLH specific in vitro monitoring were calculated by using linear regression. All statistical analyses were calculated by using GraphPad Prism (version 4.0). $P < 0.05$ was regarded as statistically significant.

ACKNOWLEDGMENTS. We thank Maichel van Riel, Eric Visser, Antoi Meeuwis, Gerty Schreibelt, Michel Olde Nordkamp, Annemiek de Boer, Nicole Scharenborg, and Mandy van der Rakt for their assistance. E.H.J.G.A. received personal Grant Agiko 2008-2-4. M.S. received personal Grant NWO VENI 700.10.409. I.J.M.d.V. received personal Grant NWO VIDI 917.76.363. This work is supported by European Grant ENCITE HEALTH-F5-2008-201842.

1. Buchbinder SP, et al.; Step Study Protocol Team (2008) Efficacy assessment of a cell-mediated immunity HIV-1 vaccine (the Step Study): A double-blind, randomised, placebo-controlled, test-of-concept trial. *Lancet* 372:1881–1893.
2. Rerks-Ngarm S, et al.; MOPH-TAVEG Investigators (2009) Vaccination with ALVAC and AIDSVAX to prevent HIV-1 infection in Thailand. *N Engl J Med* 361:2209–2220.
3. Wallis RS, et al. (2010) Biomarkers and diagnostics for tuberculosis: Progress, needs, and translation into practice. *Lancet* 375:1920–1937.
4. Kenter GG, et al. (2009) Vaccination against HPV-16 oncoproteins for vulvar intraepithelial neoplasia. *N Engl J Med* 361:1838–1847.
5. Kantoff PW, et al.; IMPACT Study Investigators (2010) Sipuleucel-T immunotherapy for castration-resistant prostate cancer. *N Engl J Med* 363:411–422.
6. Hodi FS, et al. (2010) Improved survival with ipilimumab in patients with metastatic melanoma. *N Engl J Med* 363:711–723.
7. Schwartzentruber DJ, et al. (2011) gp100 peptide vaccine and interleukin-2 in patients with advanced melanoma. *N Engl J Med* 364:2119–2127.
8. Lesterhuis WJ, Haanen JB, Punt CJ (2011) Cancer immunotherapy—revisited. *Nat Rev Drug Discov* 10:591–600.
9. Lesterhuis WJ, et al. (2008) Dendritic cell vaccines in melanoma: From promise to proof? *Crit Rev Oncol Hematol* 66:118–134.
10. Banchereau J, Palucka AK (2005) Dendritic cells as therapeutic vaccines against cancer. *Nat Rev Immunol* 5:296–306.
11. Appay V, Douek DC, Price DA (2008) CD8+ T cell efficacy in vaccination and disease. *Nat Med* 14:623–628.
12. Shields AF, et al. (1998) Imaging proliferation in vivo with [F-18]FLT and positron emission tomography. *Nat Med* 4:1334–1336.
13. Troost EG, et al. (2007) 18F-FLT PET does not discriminate between reactive and metastatic lymph nodes in primary head and neck cancer patients. *J Nucl Med* 48:726–735.
14. Fox CJ, Hammerman PS, Thompson CB (2005) Fuel feeds function: Energy metabolism and the T-cell response. *Nat Rev Immunol* 5:844–852.
15. Nair-Gill E, et al. (2010) PET probes for distinct metabolic pathways have different cell specificities during immune responses in mice. *J Clin Invest* 120:2005–2015.
16. Balch CM, et al. (2001) Final version of the American Joint Committee on Cancer staging system for cutaneous melanoma. *J Clin Oncol* 19:3635–3648.
17. de Vries IJ, et al. (2005) Immunomonitoring tumor-specific T cells in delayed-type hypersensitivity skin biopsies after dendritic cell vaccination correlates with clinical outcome. *J Clin Oncol* 23:5779–5787.
18. de Vries IJ, et al. (2005) Magnetic resonance tracking of dendritic cells in melanoma patients for monitoring of cellular therapy. *Nat Biotechnol* 23:1407–1413.
19. de Vries IJ, Adema GJ, Punt CJ, Figdor CG (2005) Phenotypical and functional characterization of clinical-grade dendritic cells. *Methods Mol Med* 109:113–126.
20. Figdor CG, de Vries IJ, Lesterhuis WJ, Melief CJ (2004) Dendritic cell immunotherapy: Mapping the way. *Nat Med* 10:475–480.
21. Schuurhuis DH, et al. (2009) In situ expression of tumor antigens by messenger RNA-electroporated dendritic cells in lymph nodes of melanoma patients. *Cancer Res* 69:2927–2934.
22. Verdijk P, et al. (2007) Sensitivity of magnetic resonance imaging of dendritic cells for in vivo tracking of cellular cancer vaccines. *Int J Cancer* 120:978–984.